The bigger picture: global analysis of solubilization performance of classical detergents versus new synthetic polymers utilizing shotgun proteomics

Stefan Mueller[a]*, Jan Kubicek[b], Felipe Merino[b], Philipp Hanisch[b], Barbara Maertens[b] and Jan-Wilm Lackmann[c]

[a]CECAD/CMMC Proteomics Facility, Center for Molecular Medicine Cologne (CMMC) Universitaet Koeln, Robert-Koch-Str. 21, 50931 Köln, Germany

[b]Cube Biotech GmbH, Creative Campus Allee 12, 40789 Monheim, Germany

[c]CECAD/CMMC Proteomics Facility, CECAD - Cluster of Excellence, Universitaet Koeln, Robert-Koch-Str. 21, 50931 Köln, Germany

*Correspondence to: stefan.mueller@uni-koeln.de

Abstract

Integral membrane proteins are critical for many cellular functions. Roughly 25% of all human genes code for membrane proteins, and about 70% of all approved drugs target them. Despite their importance, laborious and harsh purification conditions often hinder their characterization. Traditionally, they are removed from the membrane using detergents, thereby taking the proteins out of their native environment, affecting their function. Recently, a variety of synthetic polymers have been introduced, which can extract membrane proteins together with their native lipids into a so-called native nanodisc. However, they usually show lesser solubilization capacity than detergents, and their general applicability for membrane protein biochemistry is poorly understood. Here, we used Hek293 cell membrane extracts and LC-MS-based proteomics to compare the ability of nanodisc-forming polymers against state-of-the-art detergents to solubilize the membrane proteome. Our data demonstrates the general ability of synthetic co-polymers to extract membrane proteins, rivaling the efficacy of commonly used detergents. Interestingly, each class of solubilization agent presents specific solubilization profiles. We found no correlation between efficiency and number of transmembrane domains, isoelectric point, or GRAVY score for any compound. Our data shows that these polymers are a versatile alternative to detergents for the biochemical and structural study of membrane proteins, functional proteomics, or as components of native lysis/solubilization buffers. Our work here represents the first attempt at a proteome-scale comparison of the efficacy of nanodisc-forming polymers. These data should serve as starting reference for researchers looking to purify membrane proteins in near native conditions.

Introduction

Integral membrane proteins perform key cellular functions, such as cell signaling, selective transport, and more generally they mediate the interaction between cells and their environment. Although they represent about a quarter of all proteins encoded in the human genome (Fagerberg et al., 2010) they are the target of the majority of currently approved drugs (Santos et al., 2017). Despite their clear relevance, they remain very poorly characterized. For instance, up until 2021, only 3% of all structures in the PDB were membrane proteins (Le Bon et al., 2021). Many factors contribute to this, including low production yields, but perhaps the biggest challenge is that they need to be solubilized from the membrane. Traditionally, this is done using detergents, which remove the majority, if not all, lipids around the protein. Stripping membrane proteins of their native environment usually leads to instability as lipids are known to be important co-factors for protein structure and function (Barrera et al., 2013; Bogdanov et al., 2008; Contreras et al., 2011; Laganowsky et al., 2014; Pollock et al., 2018; Saliba et al., 2015; Schmidpeter et al., 2022), and detergents can replace the lipid bilayers only to a very limited extent (Seddon et al., 2004). In general, application and protein identity will determine which detergent is most appropriate. For example, quantitative and deep profiling of entire proteomes often requires either strong detergents such as sodium dodecyl sulfate (SDS), sodium deoxycholate (SDC), or RapiGest™, high concentrations of chaotropic agents such as 8 M Urea or 6 M Guanidinium Hydrochloride, or a mixture of them (Hughes et al., 2014; Vit et al., 2016; Wiśniewski et al., 2009). Furthermore, the enrichment of membranes by ultracentrifugation followed by washing with alkaline sodium carbonate or 8 M Urea has been described to improve the identification of low abundant membrane proteins (Fujiki et al., 1982; Kongpracha et al., 2022). In the case of quantitative proteomics, highly denaturing extraction conditions are extremely helpful, since they instantly reduce intrinsic protease and phosphatase activity in extracts, disrupt supramolecular protein networks and unfold proteins making them amenable for efficient tryptic digestion. In clear contrast, structural and functional characterization requires proteins in near native state, and enzymatic activity as well molecular interactions should be preserved as far as possible. While many soluble proteins can be easily extracted in simple aqueous buffers, the addition of mild detergents such as decyl maltoside (DM), dodecyl maltoside (DDM), and lauryl maltose neopentyl glycol (LMNG) (Choy et al., 2021) is required for membrane proteins. To stabilize extracted membrane proteins, detergents must be kept above their critical micelle concentration (CMC) over the entire workflow, significantly increasing reagent costs, experiment complexity, and negatively affecting many downstream applications.

More than two decades ago, the group of Jean-Luc Popot (Tribet et al., 1996) developed a new kind of amphipathic polymers or "amphipols", capable of stabilizing integral membrane proteins. Amphipols can provide the hydrophobic environment the protein needs and bind it so tightly that no additional amphipol or detergent is needed in downstream applications. For this reason, classical amphipols like A8-35, have been particularly popular for single particle electron cryo-microscopy (Cryo-EM) structures (Popot, 2018; Zoonens and Popot, 2014). Unfortunately, these polymers lack the ability to directly solubilize proteins from the membrane, and an initial detergent extraction is required. In 2009, the Overduin lab introduced a new class of co-polymer to tackle the challenge of solubilizing while preserving the native lipid environment (Knowles et al., 2009). Made by repeating units of styrene and maleic acid (SMA), SMAs were known to act as a molecular “cookie cutter” (Parmar et al., 2016). They extract integral membrane proteins together with a belt of their native lipids out of the membrane, forming a so-called Styrene and Maleic acid lipid particle (SMALP). To date, SMALPs have been used for many applications, including radioligand and spectroscopic binding assays, NMR based assays, and measurement of channel activity (see (Unger et al., 2021) for a summary). Unfortunately, SMALPs are unstable at pH values below 6.5, precipitate in the presence of divalent ions, and interfere with protein quantification using aromatic side chain absorption. However, in recent years, the promise of preserving the native lipid environment of the protein has led to the development of several alternative co-polymers that tackled some of the shortcomings of the original SMAs (for an overview of this rapidly evolving field see (Brown et al., 2021; Krishnarjuna and Ramamoorthy, 2022; Orekhov et al., 2022)). Variations in composition and manufacturing processes generate polymers with distinct capabilities. For instance, by replacing styrene with diisobutylene, Diisobutylene-maleic acid (DIBMA) produces a gentler polymer without absorption at 280 nm and higher tolerance to divalent ions (Oluwole et al., 2017). Although less efficient than SMAs, DIBMA could successfully solubilize ß2 adrenergic receptors producing a functional protein with higher stability compared to DDM (Harwood et al., 2021). Recently, two new polymer classes have been reported. Smith and colleagues (Smith et al., 2020) introduced a new co-polymers made of acrylic acid and styrene (AASTY) synthesized by reversible addition-fragmentation chain-transfer. AASTYs have a much more precisely controlled molecular weight and the use of acrylic acid confers them higher tolerance to divalent ions than SMAs (Timcenko et al., 2022). Interestingly, the group of Manuela Zoonens recently demonstrated that replacing the aliphatic group of traditional amphipols with cyclo-alkanes (CyclAPols, known commercially as Ultrasolute™ Amphipols) resulted in polymers with excellent solubilization characteristics, capable of forming native nanodiscs (Marconnet et al., 2020). Moreover, CyclAPols solubilized bacteriorhodopsin shows increased thermal stability when compared to SMAs.

94 Lipidomics analysis of SMALPs and DIBMA solubilized lipid particles has demonstrated that both polymer
95 classes can successfully extract native lipids from eukaryotic and bacterial cells, although the extracted
96 lipidic composition is to some extend dependent on the exact chemical nature of the polymer.
97 Interestingly, the lipid composition of SMALPs also depends on the identity of the protein (Teo et al.,
98 2019) suggesting that these polymers can capture local compositional variations of the membrane. For
99 most of these polymers, high-resolution Cryo-EM structures are available for membrane proteins
100 solubilized from bacterial (Catalano et al., 2021; Doyle et al., 2022; Flegler et al., 2020; Higgins et al.,
101 2021; Qiu et al., 2018; Sun et al., 2018; Swainsbury et al., 2023; Tascón et al., 2020) or eukaryotic cells
102 (Yoder and Gouaux, 2020; Yu et al., 2021), many of which showing densities consistent with the presence
103 of native lipids (Catalano et al., 2021; Doyle et al., 2022; Flegler et al., 2020; Qiu et al., 2018; Yoder and
104 Gouaux, 2020). Unfortunately, while there is clear evidence that all these polymers can form native
105 nanodiscs, most of the information about their solubilization capabilities comes from selected example
106 proteins and systematic characterization of their solubilization capacity against other methods has only
107 recently been performed for SMA (Carlson et al., 2019; Morrison et al., 2021).

108 Here, we used LC-MS analysis to compare the ability of nanodisc-forming polymers and detergents to
109 extract membrane proteins from Hek293 cells. In contrast to the in-depth characterization of selected
110 protein examples, shotgun proteomics facilitates the quantification of thousands of individual proteins in
111 parallel and allows for more generalized observations. Testing a total of 22 extraction conditions including
112 different types of SMAs, DIBMAs, AASTYs, and Ultrasolute™ Amphipol, and the commonly used non-ionic
113 detergents DM, DDM, and LMNG, our data represents the most comprehensive proteome-scale study on
114 membrane protein solubilization by polymers.

115

116 **Methods**

117 **Cell culture**

118 Human embryonic kidney 293 cells (Expi293F™, Thermo Fisher) were cultured in Expi293™ Expression
119 medium at a cell density between 5 x 10^5 cells/ml and 4 x 10^6 cells/ml in suspension. 100 ml of a 2 x 10^6
120 cells/ ml culture growing in exponential phase were harvested by centrifugation and the cell pellet was
121 stored at – 80 °C.

122

123 **Preparation of membrane pellets**

124 The cell pellet was resuspended in 150 mM NaCl and 20 mM HEPES, pH 7.4, cells were disrupted by
125 sonication. After a centrifugation step at 9,000 x g the protein concentration of the supernatant was
126 adjusted to 0.25 mg/ml using 150 mM NaCl and 20 mM HEPES pH 7.4. The adjusted supernatant was
127 pipetted into 100µl aliquots, and the aliquots centrifuged at 60,000 x g for 1 hour. The supernatant was
128 discarded and the cell pellets consisting of approximately 25 µg of total proteins were frozen at -80 °C.

129

130 **Protein extraction and digestion**

131 For an initial protein extraction screen SDS was tested as a 5% solution in 50 mM HEPES pH 7.4. RIPA
132 buffer was composed of 150 mM NaCl, 1% Nonidet P-40, 0.5% deoxycholate, and 0.1% SDS in 50 mM
133 HEPES pH 7.4. All other tested synthetic polymers and detergents were used as 2.5% solutions in 50 mM
134 HEPES pH 7.4 (Table 1). In a subsequent dilution experiment the extraction properties of a selected panel
135 of detergents and polymers were tested using five different concentrations ranging from 0.125% to 2.5%
136 in 50 mM HEPES pH 7.4 (Table 1). All reagent solutions and samples were used at 5° C and kept in pre-
137 chilled cooling racks. Either 25 µl detergent or polymer solution were added to the membrane pellets,
138 each containing approximately 25 µg total protein. The tubes were briefly vortexed and placed in a
139 Thermomixer (Eppendorf) for 16 h at 800 rpm and 5°C. After extraction, the tubes were transferred to a
140 pre-chilled rotor and centrifuged for 35 min at 21,000 x g and 5°C. 20 µl supernatant was carefully
141 transferred to new tubes without touching their bottom. 80 µl of cold acetone (-20°C) was added, the
142 tubes were briefly vortexed and incubated for 120 min at -20°C to precipitate proteins. Supernatants
143 were removed and the remaining protein pellets were washed once with 250 µl cold acetone (-20°). 25 µl
144 2% deoxycholate in 50 mM HEPES Tris HCl pH 8.5, 5 mM TCEP, and 40 mM chloroacetamide were added

145 to the airdried protein pellets. Proteins were re-solubilized, reduced and S-alkylated in a single step for 2
146 h at 46°C. 0.5 µg trypsin was added in 5 µl 2% deoxycholate in 50 mM TrisHCl pH 8.5 and proteins were
147 digested at 37°C. After 16 h, 30 µl of 5% trifluoroacetic acid was added to stop the digestion. By following
148 this precipitation-resolubilization protocol, we removed solubilization agents and standardize the tryptic
149 digestion step, which is fully compatible with SDC (Lin et al., 2008). Samples were centrifuged for 5 min at
150 21,000 x g and 20°C to pellet precipitated deoxycholate and 50 µl clear supernatant was removed and
151 transferred to fresh tubes. 20 µl were subsequently loaded on DVB-RPS mixed mode stage tips activated
152 with 20 µl methanol and equilibrated to 0.1% formic acid (FA). The loaded peptides were sequentially
153 washed with 40 µl 0.1% FA in water and 40 µl 0.1% FA in 60% acetonitrile followed by alkaline elution
154 with 40 µl 1% ammonium hydroxide in 60% acetonitrile. Eluates were immediately acidified with 10 µl
155 10% FA and dried in a vacuum centrifuge. Samples were re-solubilized in 10 µl 5% FA, 2% acetonitrile, and
156 stored at -20°C until LC-MS analysis.

157

158 **LC-MS Data acquisition and processing**

159 Protein digests were analyzed on a Q-Exactive Plus (Thermo Scientific) mass spectrometer that was
160 coupled to an EASY nLC 1200 UPLC (Thermo Scientific). Re-solubilized protein digests were loaded onto
161 an in-house-made pulled tip column (30 cm length, 75 µm inner diameter, filled with 2.7 µm Poroshell
162 EC120 C18, Agilent) which has been equilibrated in 0.1% FA in water. Peptides were separated using
163 increasing acetonitrile concentrations in 0.1% FA followed by a 10 min column wash with 95% acetonitrile
164 in 0.1 % FA. 140 min gradients were used for data dependent (DDA) acquisitions and 90 min gradients
165 with data independent (DIA) acquisitions. The protein extraction screen experiment was acquired with
166 the DDA method. Briefly, MS1 survey scans were acquired from 300 to 1,750 m/z at a resolution of
167 70,000 and stored in profile mode. The top 10 most abundant peptides were isolated within a 1.8 Th
168 window and subjected to HCD fragmentation at a normalized collision energy setting of 27%. The AGC
169 target was set to 5e5 charges, allowing a maximum injection time of 60 ms. Product ions were detected
170 in the Orbitrap at a resolution of 17,500. Precursors were dynamically excluded for 25 s. A DIA method
171 was used for the analysis of the dilution experiment. MS1 scans were acquired from 380 m/z to 1,020
172 m/z at 35,000 resolution. Maximum injection time was set to 60 ms and the AGC target to 1E6. MS2
173 scans starting from 250 m/z were acquired with 17,500 resolution, maximum injection time of 60 ms,
174 and the AGC target set to 1E6. 30 x 20 m/z staggered DIA windows covered the precursor mass range
175 from 400 m/z – 1,000 m/z and resulted in 60 nominal 10 m/z windows after deconvolution. For spectral

176 library generation, aliquots of the 2.5% condition of all extraction experiments were pooled and analyzed
177 with six consecutive gas phase fractionation (GPF) runs covering the mass range from 400 m/z to 1,000
178 m/z in sequential 100 m/z segments. MS2 scans were acquired with 25 x 4 m/z staggered windows in a
179 100 m/z range. All other settings were identical to the standard DIA method used for sample acquisition.
180 DDA and DIA data were stored as centroid.

181

182 **Data analysis**

183 DDA runs were processed with MaxQuant version 1.5.3.8 (Tyanova et al., 2016a) using default
184 parameters. Briefly, MS2 spectra were searched against the human canonical Swissprot reference
185 proteome database (UP5640, downloaded 08/26/2020), including a list of common contaminants. False
186 discovery rates on protein and PSM level were estimated by the target-decoy approach to 1% Protein
187 FDR and 1% PSM FDR respectively. The minimal peptide length was set to 7 amino acids and
188 carbamidomethylation at cysteine residues was considered as a fixed modification. Oxidation (M) and
189 Acetyl (Protein N-term) were included as variable modifications. The "match between runs" option was
190 enabled within replicate groups. Protein and gene identifiers together with iBAQ intensities were
191 imported into Perseus version 1.6.5.0 (Tyanova et al., 2016b) for subsequent analysis. Decoys and
192 potential contaminants were removed. iBAQ values were log2 transformed and identified proteins were
193 filtered for at least 3 out of 3 values in at least one replicate group. The number of transmembrane
194 domains (TMDs) together with start and end points of corresponding TMD sequence stretches were
195 extracted from Uniprot for each protein and merged to the data set. Principal component analysis was
196 calculated on the imputed group means using Perseus defaults. Hek293 gene expression data were
197 downloaded from https://www.proteinatlas.org (Uhlén et al., 2015). Entries with transcripts per million
198 (TPM) below 1 were considered to be noise level and removed together with non-membrane proteins
199 (TMD count = 0). Remaining entries were considered as expected membrane protein expression
200 background. Grouped mean iBAQ intensities as well as protein level TMD counts were merged to the
201 expression background and the percentage of entries that were also identified by the proteomics
202 experiment was calculated to estimate the analytical depth of the proteomic analysis. Gravy Scores and
203 Isoelectric points were calculated from the human canonical Swissprot database proteome (UP5640)
204 using the "Peptides" R-package (https://github.com/dosorio/Peptides/).

205 All DIA raw files were deconvoluted and transformed to mzML files using the msconvert module in
206 Proteowizard. DIA-NN 1.8.0 (Demichev et al., 2020) was used in library free mode to generate a project

207 specific spectral library from a human canonical Swissprot reference proteome fasta file and the six GPF
208 runs. The settings differing from defaults were: min precursor m/z set to 400, max precursor m/z set to
209 1,000, min fragment m/z set to 250, max fragment m/z set to 1,800, and precursor charge states ranging
210 from 2 to 4. The resulting spectral library (11,214 proteins, 11,186 genes and 139,723 precursors) was
211 used for the subsequent analysis of the sample runs with default parameters and the relaxed protein
212 inference option. Using the "diann" R-package (https://github.com/vdemichev/diann-rpackage). MaxLFQ
213 intensities were calculated from non-normalized intensities provided in the DIA-NN output file and were
214 imported into Perseus. For heatmap generation, log2 transformed MaxLFQ values were normalized to an
215 interval from 0-1.

216 **Results and Discussion**

217 We used LC-MS to compare a panel of nanodisc-forming polymers and commonly used detergents for
218 their ability to extract integral transmembrane proteins from Hek293 cell membranes. In total 22
219 extraction conditions including different types of SMAs, DIBMAs, AASTYs, and Ultrasolute™ Amphipols,
220 and the commonly used non-ionic detergents DM, DDM, and LMNG were tested. Our non-detergent
221 control was HEPES buffer. As positive control we chose SDS, SDC, and Fos-12 as a panel of very aggressive
222 detergents, as well as the ubiquitously used RIPA buffer. While these are not suited for native extraction,
223 their high protein solubilization capacity should provide an upper limit of detectable membrane proteins
224 in the current experimental setup. For an overview of the compounds tested (Table 1) and their
225 physicochemical characteristics see Table S1.

226

227 **Analytical depth of our study**

228 We could identify a total of 7,197 proteins across all runs, including 5,665 non-membrane proteins (Table
229 S2). We attribute this to loosely membrane-interacting proteins or soluble proteins trapped in vesicles.
230 Normally, this is dealt with by washing the samples with alkaline carbonate buffers (Fujiki et al., 1982;
231 Kongpracha et al., 2022). However, the elevated pH needed for this (> 11) is incompatible with native
232 protein extraction. Therefore, we filtered the data for proteins with at least one trans membrane domain
233 (TMD), leaving 1,532 membrane protein identifications. For comparison, RNA-seq experiments of Hek293
234 cells report 2,371 transmembrane proteins to be expressed with transcript levels greater than 1
235 transcript per million (Protein Atlas; https://www.proteinatlas.org/). Considering this number as
236 expression background, we estimated the analytical depth of our proteome analysis to be better than 64
237 % for proteins with at least one TMD. Importantly, while mRNA levels are not always good predictors of
238 protein amounts, they should be strongly correlated with the cell growth conditions we tested (Liu et al.,
239 2016). Indeed, comparing transcript levels with our detected proteins (Figure S1), suggests that low gene
240 expression is the major reason for proteins missing in our data set, strongly arguing for the high quality of
241 the dataset.

242

243 **Different solubilization compounds result in unique solubilization patterns**

244 For our initial screening round, we assessed the solubilization capacity of all compounds at a final
245 concentration of 2.5%, or 5% in the case of SDS. To get an initial overview of their solubilization

246 differences, we used the mean abundance of the detected membrane proteins to perform a principal
247 component analysis (PCA). Strikingly, the first two components (~70% of the variance) reveal that
248 individual reagents form tight clusters with other members of their respective classes (Figure 1A). Higher
249 components can separate ionic from non-ionic detergents, while to a lesser extent still preserving the
250 separate clustering of the different polymer classes (Figure 1B)

251 The clear separation between detergents and polymers, as well as the separation between different
252 polymer classes suggest that each solubilization agent class produces a distinctive fingerprint. However, a
253 relation between the individual components of the PCA and the specific physicochemical characteristics
254 of the compounds is not immediately obvious. To our surprise, although denaturation potential and
255 extraction properties of ionic and non-ionic detergents are clearly different, DM, DDM, and LMNG cluster
256 closely with the much more aggressive SDS, SDC, and Fos-12. As expected, the RIPA buffer — a mixture of
257 SDS, SDC, and Nonidet P-40 (NP-40) — is located within this cluster as well. Digitonin does not follow this
258 trend and is located far away from the main detergent cluster, near SMA 502-E.

259

260 **Polymers can efficiently solubilize membrane proteins**

261 Next, we sought to understand whether the differences in solubilization profiles we observe are a
262 consequence of differences in solubilization efficiency or versatility. In our negative control, we detected
263 an average of 253 membrane proteins, 181 (71.41%) of which are single span membrane proteins (Figure
264 2). In clear contrast, the membrane protein counts for the ionic detergents SDC, SDS, and Fos-12 were
265 1250, 1,241, and 1,280 respectively. Unexpectedly, the ionic detergents performed similarly to
266 Ultrasolute™ Amphipol-17 and Amphipol-18 (1,270 and 1,272 membrane proteins respectively) and
267 were outperformed by the non-ionic detergents DM, DDM, and LMNG (membrane protein counts of
268 1,297, 1,308, and 1,315 respectively); the latter being the highest in the data set (Figure 2). We obtained
269 intermediate efficiency for SMAs, with counts of 1,175, 1,198, and 1,066 for SMA-200, SMA-300, and
270 SMA-502-E respectively. AASTYs and the DIBMAs had the lowest performance with counts ranging from
271 991 to 1,010 and from 897 to 969 respectively (Figure 2). Nevertheless, DIBMAs and AASTYs are efficient
272 solubilization agents, showing significantly higher solubilization than the background HEPES alone.
273 Importantly, solubilization efficiency of membrane proteins is only one piece of the puzzle. Purification
274 strategy, stabilization of the membrane protein, and downstream applications are equally important
275 aspects to consider, which makes screening of various reagents indispensable. Indeed, polymer identity
276 or even concentration can affect all of these parameters (Szundi et al., 2021). Absolute solubilization

277 efficiency may also not be critical for many applications where a near-native state is the strongest
278 constraint and sufficient initial material is present; the obvious example would be after overexpression.
279 For instance, the comparably milder DIBMA has been successfully used to determine the Cryo-EM
280 structure of the mechanosensitive-like channel YnaI (Flegler et al., 2020) and has been successfully used
281 to produce highly active and stable GPCR samples (Harwood et al., 2021).

282

283 **Polymers can efficiently extract diverse classes of membrane proteins**

284 Our PCA analysis revealed that the different compound classes we tested produce distinct solubilization
285 patterns. Although they clearly differ in their solubilization efficiency, this cannot be the only driver as the
286 clustering of detergent and polymer classes remains present for higher components in the PCA analysis
287 (Figure 1B). We first analyzed the potential impact of the membrane protein topology on solubilization.
288 For this, we grouped proteins according to their number of TMDs and calculated identification rates as
289 the fraction of membrane proteins we identified versus what we expected from RNA data. Identification
290 rate differs substantially among TMD groups (Figure 3). Interestingly, the profiles are similar for all tested
291 extraction conditions, with scale differences clearly proportional to efficiency. Since median protein
292 abundancies have a major impact on identification rates in proteomic experiments, we tested if this was
293 behind the identification rate pattern. Indeed, the mRNA level shows a similar pattern to our detection
294 rates (Figure 3), with a significant correlation between identification rates and median mRNA abundance
295 (Figure S1). In turn, this suggests that protein abundance and not preferential solubilization is behind the
296 identification rate pattern across the TMD groups.

297 A clear candidate for the differential polymer preferences would be the physicochemical properties of
298 the proteins and their respective transmembrane regions. For instance, hydrophobicity and charge
299 substantially differ across membrane proteins and could easily affect the polymer's solubilization
300 efficiency. To test this, we calculated GRAVY scores and isoelectric points for either the full protein
301 sequences or their membrane spanning regions. Interestingly, the distributions of either characteristic for
302 the detected membrane proteins reveal no major difference among the solubilization agents, strongly
303 suggesting that isoelectric points and hydrophobicity cannot explain the differential extraction patterns
304 that we observe (Figure 4).

305 Contrary to detergents, the polymers we tested solubilize the protein together with its lipidic
306 microenvironment. Far from being just a scaffold for these proteins, the exact lipidic environment around
307 them is matched to their specific requirements (Lee, 2004), with each of them possessing its own lipidic

308 fingerprint (Corradi et al., 2018). Interestingly, SMAs have already been shown to solubilize, from the
309 same membrane, proteins with different local lipidic compositions (Teo et al., 2019). However, early
310 characterization of nanodisc-forming polymers has shown that their solubilization efficiency is somehow
311 dependent on membrane composition (Oluwole et al., 2017; Smith et al., 2020). Combined, this suggests
312 that, for a specific target, differences in solubilization ability between polymers would be partially
313 determined by the identity of the annular lipids surrounding the membrane protein.

314

315 **Optimal solubilization conditions are specific to each compound and target combination**

316 So far, we compared the capacity of polymers and detergents to extract membrane proteins using a
317 standard concentration of 2.5%. Although this concentration is effective for all conditions tested, it is
318 relatively high. In many cases, high concentrations like these can interfere with purification, or affect the
319 activity of the protein (Szundi et al., 2021). In those kinds of cases where gentle solubilization of proteins
320 is required, it is common practice to use additives at concentrations as low as possible in order to
321 minimize detrimental effects. DDM and LMNG are typically used from 0.1% to 1%**,** whereas SMAs have
322 been successfully used in concentrations as low as 0.25% (Kopf et al., 2020; Pitch et al., 2021). In order to
323 determine useful minimal concentrations, we performed a second extraction screen with concentrations
324 of 0.125%, 0.25%, 0.5%, 1%, and 2.5% for a selected panel of polymers and non-ionic detergents. Protein
325 identifications and quantities from this experiment can be found in Table S2**.** In line with the first
326 screening, DDM and LMNG were the most efficient compounds and reached maximum membrane
327 protein counts at concentrations as low as 0.5% (Figure 5A) and maximum summed intensities at 1%
328 (Figure 5B). In agreement with our earlier experiments, Ultrasolute™ Amphipol-17 and -18 showed very
329 high solubilization efficiency reaching their maximum counts at 1% and plateauing at a maximum value of
330 summed intensities comparable to detergents. AASTY 11-45 and 6-50 also reached a plateau for summed
331 intensities at concentrations above 1%, although only AASTY 11-45 does not seem to find a plateau for
332 the number of individual membrane proteins (Figure 5A,B). DIBMAs in general seem to find a plateau for
333 both quantities, although with much lower values (Figure 5A,B), arguing for a generally lower
334 solubilization efficiency. For all other compounds, the curves imply that the concentration for maximum
335 solubilization has not been reached and may clearly exceed 2.5%. Combined, this shows that polymers
336 can be efficiently used at concentrations significantly lower than 2.5%. We would recommend 0.25 – 1%
337 for Ultrasolute™ Amphipols and 0.5 – 1% for AASTYs, while a higher concentration would be required for

338 DIBMAs and SMAs. To what extent these results from endogenously expressed targets in this study can
339 be transferred to overexpression conditions has to be tested individually for each target.

340 Finally, to further dissect the versatility of these polymers we created a heatmap of the relative protein
341 intensities obtained for each individual detected membrane protein, at each different solubilization agent
342 concentration (Figure 6). Unsurprisingly, detergents are able to solubilize most of the proteins in the map
343 with high efficiency. In addition, Ultrasolute™ Amphipols and to a lesser extent AASTY 6-50 produce a
344 very similar pattern, both in terms of concentration dependency and number and identity of the
345 solubilized proteins. Combined this demonstrates that nanodisc-forming polymers present a strong
346 alternative to detergents, especially when the lipid environment is key for protein function.

347

348 **Concluding remarks**

349 We used LC-MS to perform label-free quantification proteomics aimed at screening native-nanodisc-
350 forming polymers and compared them with state-of-the-art detergents for their ability to solubilize the
351 Hek293 membrane proteome. We omitted other membrane-mimetic strategies — such as MSP-based
352 nanodisc (Bayburt et al., 2002), peptidisc (Carlson et al., 2018), and saponins (Frauenfeld et al., 2016) —
353 as they all require the intermediate addition of detergents, thus altering the native environment of the
354 proteins under investigation. The study presented here is the first major attempt to compare the ability
355 of a comprehensive panel of polymers at the membrane proteome scale. As such, we believe that this
356 study will become a reference for researchers working with different aspects of the biochemistry of
357 membrane proteins.

358 We have demonstrated that these synthetic polymers exhibit solubilization performance that can rival
359 those observed in commonly used detergents, but have the advantage of preserving the protein in a
360 near-native environment; Ultrasolute™ Amphiphol 17 and 18 were as efficient as the denaturing
361 detergent group. Considering the separate clustering observed in Figure 1, plus the patterns observed in
362 Figure 6, we believe that, for any given target, it is likely that at least one polymer class should provide
363 efficient solubilization. We are certain that the ability to preserve the native membrane environment will
364 become and invaluable tool for membrane biochemists. As such, we anticipate that these synthetic
365 polymers will have a broad range of applications in the future, in particular as components of native lysis
366 and solubilization buffers. Moreover, with the ever-increasing access the electron cryo-microscopy we
367 expect that these polymers will make a big impact in the structural biology of integral membrane
368 proteins.

Acknowledgments

All mass spectrometric analysis was performed in the CMMC/CECAD Proteomics Facility, CECAD University of Cologne.

Data Availability

The results of the mass spectrometry data included in this manuscript is available in Table S2.

Conflict of interest disclosure

JK, BM, PH, and FM are shareholders of Cube Biotech GmbH, which produces and sells synthetic co-polymers for membrane protein characterization. SM and JWL declare no conflict of interest.

381 **References**

382 Barrera, N.P., Zhou, M., Robinson, C.V., 2013. The role of lipids in defining membrane protein interactions:
383 insights from mass spectrometry. Trends Cell Biol. 23, 1–8. https://doi.org/10.1016/j.tcb.2012.08.007

384 Bogdanov, M., Mileykovskaya, E., Dowhan, W., 2008. Lipids in the Assembly of Membrane Proteins and
385 Organization of Protein Supercomplexes. Subcell. Biochem. 49, 197–239. https://doi.org/10.1007/978-1-
386 4020-8831-5_8

387 Brown, C.J., Trieber, C., Overduin, M., 2021. Structural biology of endogenous membrane protein
388 assemblies in native nanodiscs. Curr. Opin. Struct. Biol. 69, 70–77.
389 https://doi.org/10.1016/j.sbi.2021.03.008

390 Carlson, M.L., Stacey, R.G., Young, J.W., Wason, I.S., Zhao, Z., Rattray, D.G., Scott, N., Kerr, C.H., Babu, M.,
391 Foster, L.J., Duong Van Hoa, F., 2019. Profiling the Escherichia coli membrane protein interactome
392 captured in Peptidisc libraries. eLife 8, e46615. https://doi.org/10.7554/eLife.46615

393 Catalano, C., Ben-Hail, D., Qiu, W., Blount, P., des Georges, A., Guo, Y., 2021. Cryo-EM Structure of
394 Mechanosensitive Channel YnaI Using SMA2000: Challenges and Opportunities. Membranes 11, 849.
395 https://doi.org/10.3390/membranes11110849

396 Choy, B.C., Cater, R.J., Mancia, F., Pryor, E.E., 2021. A 10-year meta-analysis of membrane protein
397 structural biology: Detergents, membrane mimetics, and structure determination techniques. Biochim.
398 Biophys. Acta BBA - Biomembr. 1863, 183533. https://doi.org/10.1016/j.bbamem.2020.183533

399 Contreras, F.-X., Ernst, A.M., Wieland, F., Brügger, B., 2011. Specificity of Intramembrane Protein–Lipid
400 Interactions. Cold Spring Harb. Perspect. Biol. 3, a004705. https://doi.org/10.1101/cshperspect.a004705

401 Corradi, V., Mendez-Villuendas, E., Ingólfsson, H.I., Gu, R.-X., Siuda, I., Melo, M.N., Moussatova, A.,
402 DeGagné, L.J., Sejdiu, B.I., Singh, G., Wassenaar, T.A., Delgado Magnero, K., Marrink, S.J., Tieleman, D.P.,
403 2018. Lipid–Protein Interactions Are Unique Fingerprints for Membrane Proteins. ACS Cent. Sci. 4, 709–
404 717. https://doi.org/10.1021/acscentsci.8b00143

405 Demichev, V., Messner, C.B., Vernardis, S.I., Lilley, K.S., Ralser, M., 2020. DIA-NN: neural networks and
406 interference correction enable deep proteome coverage in high throughput. Nat. Methods 17, 41–44.
407 https://doi.org/10.1038/s41592-019-0638-x

408 Doyle, M.T., Jimah, J.R., Dowdy, T., Ohlemacher, S.I., Larion, M., Hinshaw, J.E., Bernstein, H.D., 2022. Cryo-
409 EM structures reveal multiple stages of bacterial outer membrane protein folding. Cell 185, 1143-
410 1156.e13. https://doi.org/10.1016/j.cell.2022.02.016

411 Flegler, V.J., Rasmussen, A., Rao, S., Wu, N., Zenobi, R., Sansom, M.S.P., Hedrich, R., Rasmussen, T.,
412 Böttcher, B., 2020. The MscS-like channel YnaI has a gating mechanism based on flexible pore helices.
413 Proc. Natl. Acad. Sci. 117, 28754–28762. https://doi.org/10.1073/pnas.2005641117

414 Fujiki, Y., Hubbard, A.L., Fowler, S., Lazarow, P.B., 1982. Isolation of intracellular membranes by means of
415 sodium carbonate treatment: application to endoplasmic reticulum. J. Cell Biol. 93, 97–102.
416 https://doi.org/10.1083/jcb.93.1.97

417 Harwood, C.R., Sykes, D.A., Hoare, B.L., Heydenreich, F.M., Uddin, R., Poyner, D.R., Briddon, S.J.,
418 Veprintsev, D.B., 2021. Functional solubilization of the β2-adrenoceptor using diisobutylene maleic acid.
419 iScience 24. https://doi.org/10.1016/j.isci.2021.103362

420 Higgins, A.J., Flynn, A.J., Marconnet, A., Musgrove, L.J., Postis, V.L.G., Lippiat, J.D., Chung, C., Ceska, T.,
421 Zoonens, M., Sobott, F., Muench, S.P., 2021. Cycloalkane-modified amphiphilic polymers provide direct
422 extraction of membrane proteins for CryoEM analysis. Commun. Biol. 4, 1–9.
423 https://doi.org/10.1038/s42003-021-02834-3

424 Hughes, C.S., Foehr, S., Garfield, D.A., Furlong, E.E., Steinmetz, L.M., Krijgsveld, J., 2014. Ultrasensitive
425 proteome analysis using paramagnetic bead technology. Mol. Syst. Biol. 10, 757.
426 https://doi.org/10.15252/msb.20145625

427 Knowles, T.J., Finka, R., Smith, C., Lin, Y.-P., Dafforn, T., Overduin, M., 2009. Membrane Proteins
428 Solubilized Intact in Lipid Containing Nanoparticles Bounded by Styrene Maleic Acid Copolymer. J. Am.
429 Chem. Soc. 131, 7484–7485. https://doi.org/10.1021/ja810046q

430 Kongpracha, P., Wiriyasermkul, P., Isozumi, N., Moriyama, S., Kanai, Y., Nagamori, S., 2022. Simple But
431 Efficacious Enrichment of Integral Membrane Proteins and Their Interactions for In-Depth Membrane
432 Proteomics. Mol. Cell. Proteomics 21. https://doi.org/10.1016/j.mcpro.2022.100206

433 Kopf, A.H., Dörr, J.M., Koorengevel, M.C., Antoniciello, F., Jahn, H., Killian, J.A., 2020. Factors influencing
434 the solubilization of membrane proteins from Escherichia coli membranes by styrene–maleic acid
435 copolymers. Biochim. Biophys. Acta BBA - Biomembr. 1862, 183125.
436 https://doi.org/10.1016/j.bbamem.2019.183125

437 Krishnarjuna, B., Ramamoorthy, A., 2022. Detergent-Free Isolation of Membrane Proteins and Strategies
438 to Study Them in a Near-Native Membrane Environment. Biomolecules 12, 1076.
439 https://doi.org/10.3390/biom12081076

440 Laganowsky, A., Reading, E., Allison, T.M., Ulmschneider, M.B., Degiacomi, M.T., Baldwin, A.J., Robinson,
441 C.V., 2014. Membrane proteins bind lipids selectively to modulate their structure and function. Nature
442 510, 172–175. https://doi.org/10.1038/nature13419

443 Le Bon, C., Michon, B., Popot, J.-L., Zoonens, M., 2021. Amphipathic environments for determining the
444 structure of membrane proteins by single-particle electron cryo-microscopy. Q. Rev. Biophys. 54, e6.
445 https://doi.org/10.1017/S0033583521000044

446 Lee, A.G., 2004. How lipids affect the activities of integral membrane proteins. Biochim. Biophys. Acta
447 BBA - Biomembr. 1666, 62–87. https://doi.org/10.1016/j.bbamem.2004.05.012

448 Lin, Y., Zhou, J., Bi, D., Chen, P., Wang, X., Liang, S., 2008. Sodium-deoxycholate-assisted tryptic digestion
449 and identification of proteolytically resistant proteins. Anal. Biochem. 377, 259–266.
450 https://doi.org/10.1016/j.ab.2008.03.009

451 Liu, Y., Beyer, A., Aebersold, R., 2016. On the Dependency of Cellular Protein Levels on mRNA Abundance.
452 Cell 165, 535–550. https://doi.org/10.1016/j.cell.2016.03.014

453 Marconnet, A., Michon, B., Le Bon, C., Giusti, F., Tribet, C., Zoonens, M., 2020. Solubilization and
454 Stabilization of Membrane Proteins by Cycloalkane-Modified Amphiphilic Polymers. Biomacromolecules
455 21, 3459–3467. https://doi.org/10.1021/acs.biomac.0c00929

456 Morrison, K.A., Heesom, K.J., Edler, K.J., Doutch, J., Price, G.J., Koumanov, F., Whitley, P., 2021.
457 Development of Methodology to Investigate the Surface SMALPome of Mammalian Cells. Front. Mol.
458 Biosci. 8.

459 Oluwole, A.O., Danielczak, B., Meister, A., Babalola, J.O., Vargas, C., Keller, S., 2017. Solubilization of
460 Membrane Proteins into Functional Lipid-Bilayer Nanodiscs Using a Diisobutylene/Maleic Acid
461 Copolymer. Angew. Chem. Int. Ed. 56, 1919–1924. https://doi.org/10.1002/anie.201610778

462 Orekhov, P.S., Bozdaganyan, M.E., Voskoboynikova, N., Mulkidjanian, A.Y., Karlova, M.G., Yudenko, A.,
463 Remeeva, A., Ryzhykau, Y.L., Gushchin, I., Gordeliy, V.I., Sokolova, O.S., Steinhoff, H.-J., Kirpichnikov, M.P.,
464 Shaitan, K.V., 2022. Mechanisms of Formation, Structure, and Dynamics of Lipoprotein Discs Stabilized by
465 Amphiphilic Copolymers: A Comprehensive Review. Nanomaterials 12, 361.
466 https://doi.org/10.3390/nano12030361

467 Parmar, M.J., Lousa, C.D.M., Muench, S.P., Goldman, A., Postis, V.L.G., 2016. Artificial membranes for
468 membrane protein purification, functionality and structure studies. Biochem. Soc. Trans. 44, 877–882.
469 https://doi.org/10.1042/BST20160054

470 Pitch, S.G., Yao, W., Szundi, I., Fay, J., Chen, E., Shumate, A., Kliger, D.S., Farrens, D.L., 2021. Functional
471 integrity of membrane protein rhodopsin solubilized by styrene-maleic acid copolymer. Biophys. J. 120,
472 3508–3515. https://doi.org/10.1016/j.bpj.2021.05.008

473 Pollock, N.L., Lee, S.C., Patel, J.H., Gulamhussein, A.A., Rothnie, A.J., 2018. Structure and function of
474 membrane proteins encapsulated in a polymer-bound lipid bilayer. Biochim. Biophys. Acta BBA -
475 Biomembr., Beyond the Structure-Function Horizon of Membrane Proteins 1860, 809–817.
476 https://doi.org/10.1016/j.bbamem.2017.08.012

477 Popot, J.-L., 2018. Membrane Proteins in Aqueous Solutions, Biological and Medical Physics, Biomedical
478 Engineering. Springer International Publishing, Cham. https://doi.org/10.1007/978-3-319-73148-3

479 Qiu, W., Fu, Z., Xu, G.G., Grassucci, R.A., Zhang, Y., Frank, J., Hendrickson, W.A., Guo, Y., 2018. Structure
480 and activity of lipid bilayer within a membrane-protein transporter. Proc. Natl. Acad. Sci. 115, 12985–
481 12990. https://doi.org/10.1073/pnas.1812526115

482 Saliba, A.-E., Vonkova, I., Gavin, A.-C., 2015. The systematic analysis of protein–lipid interactions comes of
483 age. Nat. Rev. Mol. Cell Biol. 16, 753–761. https://doi.org/10.1038/nrm4080

484 Santos, R., Ursu, O., Gaulton, A., Bento, A.P., Donadi, R.S., Bologa, C.G., Karlsson, A., Al-Lazikani, B.,
485 Hersey, A., Oprea, T.I., Overington, J.P., 2017. A comprehensive map of molecular drug targets. Nat. Rev.
486 Drug Discov. 16, 19–34. https://doi.org/10.1038/nrd.2016.230

487 Schmidpeter, P.A.M., Wu, D., Rheinberger, J., Riegelhaupt, P.M., Tang, H., Robinson, C.V., Nimigean, C.M.,
488 2022. Anionic lipids unlock the gates of select ion channels in the pacemaker family. Nat. Struct. Mol.
489 Biol. 1–9. https://doi.org/10.1038/s41594-022-00851-2

490 Seddon, A.M., Curnow, P., Booth, P.J., 2004. Membrane proteins, lipids and detergents: not just a soap
491 opera. Biochim. Biophys. Acta BBA - Biomembr., Lipid-Protein Interactions 1666, 105–117.
492 https://doi.org/10.1016/j.bbamem.2004.04.011

493 Smith, A.A.A., Autzen, H.E., Faust, B., Mann, J.L., Muir, B.W., Howard, S., Postma, A., Spakowitz, A.J.,
494 Cheng, Y., Appel, E.A., 2020. Lipid Nanodiscs via Ordered Copolymers. Chem 6, 2782–2795.
495 https://doi.org/10.1016/j.chempr.2020.08.004

496 Sun, C., Benlekbir, S., Venkatakrishnan, P., Wang, Y., Hong, S., Hosler, J., Tajkhorshid, E., Rubinstein, J.L.,
497 Gennis, R.B., 2018. Structure of the alternative complex III in a supercomplex with cytochrome oxidase.
498 Nature 557, 123–126. https://doi.org/10.1038/s41586-018-0061-y

499 Swainsbury, D.J.K., Hawkings, F.R., Martin, E.C., Musiał, S., Salisbury, J.H., Jackson, P.J., Farmer, D.A.,
500 Johnson, M.P., Siebert, C.A., Hitchcock, A., Hunter, C.N., 2023. Cryo-EM structure of the four-subunit
501 Rhodobacter sphaeroides cytochrome bc1 complex in styrene maleic acid nanodiscs. Proc. Natl. Acad.
502 Sci. 120, e2217922120. https://doi.org/10.1073/pnas.2217922120

503 Szundi, I., Pitch, S.G., Chen, E., Farrens, D.L., Kliger, D.S., 2021. Styrene-maleic acid copolymer effects on
504 the function of the GPCR rhodopsin in lipid nanoparticles. Biophys. J. 120, 4337–4348.
505 https://doi.org/10.1016/j.bpj.2021.09.012

506 Tascón, I., Sousa, J.S., Corey, R.A., Mills, D.J., Griwatz, D., Aumüller, N., Mikusevic, V., Stansfeld, P.J., Vonck,
507 J., Hänelt, I., 2020. Structural basis of proton-coupled potassium transport in the KUP family. Nat.
508 Commun. 11, 626. https://doi.org/10.1038/s41467-020-14441-7

509 Teo, A.C.K., Lee, S.C., Pollock, N.L., Stroud, Z., Hall, S., Thakker, A., Pitt, A.R., Dafforn, T.R., Spickett, C.M.,
510 Roper, D.I., 2019. Analysis of SMALP co-extracted phospholipids shows distinct membrane environments
511 for three classes of bacterial membrane protein. Sci. Rep. 9, 1813. https://doi.org/10.1038/s41598-018-
512 37962-0

513 Timcenko, M., Autzen, A.A.A., Autzen, H.E., 2022. Characterization of Divalent Cation Interactions with
514 AASTY Nanodiscs. ACS Appl. Polym. Mater. 4, 1071–1083. https://doi.org/10.1021/acsapm.1c01507

515 Tribet, C., Audebert, R., Popot, J.-L., 1996. Amphipols: Polymers that keep membrane proteins soluble in
516 aqueous solutions. Proc. Natl. Acad. Sci. 93, 15047–15050. https://doi.org/10.1073/pnas.93.26.15047

517 Tyanova, S., Temu, T., Cox, J., 2016a. The MaxQuant computational platform for mass spectrometry-
518 based shotgun proteomics. Nat. Protoc. 11, 2301–2319. https://doi.org/10.1038/nprot.2016.136

519 Tyanova, S., Temu, T., Sinitcyn, P., Carlson, A., Hein, M.Y., Geiger, T., Mann, M., Cox, J., 2016b. The Perseus
520 computational platform for comprehensive analysis of (prote)omics data. Nat. Methods 13, 731–740.
521 https://doi.org/10.1038/nmeth.3901

522 Uhlén, M., Fagerberg, L., Hallström, B.M., Lindskog, C., Oksvold, P., Mardinoglu, A., Sivertsson, Å., Kampf,
523 C., Sjöstedt, E., Asplund, A., Olsson, I., Edlund, K., Lundberg, E., Navani, S., Szigyarto, C.A.-K., Odeberg, J.,
524 Djureinovic, D., Takanen, J.O., Hober, S., Alm, T., Edqvist, P.-H., Berling, H., Tegel, H., Mulder, J., Rockberg,
525 J., Nilsson, P., Schwenk, J.M., Hamsten, M., von Feilitzen, K., Forsberg, M., Persson, L., Johansson, F.,
526 Zwahlen, M., von Heijne, G., Nielsen, J., Pontén, F., 2015. Tissue-based map of the human proteome.
527 Science 347, 1260419. https://doi.org/10.1126/science.1260419

528 Unger, L., Ronco-Campaña, A., Kitchen, P., Bill, R.M., Rothnie, A.J., 2021. Biological insights from SMA-
529 extracted proteins. Biochem. Soc. Trans. 49, 1349–1359. https://doi.org/10.1042/BST20201067

530 Vit, O., Man, P., Kadek, A., Hausner, J., Sklenar, J., Harant, K., Novak, P., Scigelova, M., Woffendin, G.,
531 Petrak, J., 2016. Large-scale identification of membrane proteins based on analysis of trypsin-protected
532 transmembrane segments. J. Proteomics 149, 15–22. https://doi.org/10.1016/j.jprot.2016.03.016

533 Wiśniewski, J.R., Zougman, A., Nagaraj, N., Mann, M., 2009. Universal sample preparation method for
534 proteome analysis. Nat. Methods 6, 359–362. https://doi.org/10.1038/nmeth.1322

535 Yoder, N., Gouaux, E., 2020. The His-Gly motif of acid-sensing ion channels resides in a reentrant 'loop'
536 implicated in gating and ion selectivity. eLife 9, e56527. https://doi.org/10.7554/eLife.56527

537 Yu, J., Zhu, H., Lape, R., Greiner, T., Du, J., Lü, W., Sivilotti, L., Gouaux, E., 2021. Mechanism of gating and
538 partial agonist action in the glycine receptor. Cell 184, 957-968.e21.
539 https://doi.org/10.1016/j.cell.2021.01.026

540 Zoonens, M., Popot, J.-L., 2014. Amphipols for Each Season. J. Membr. Biol. 247, 759–796.
541 https://doi.org/10.1007/s00232-014-9666-8

542

543 **Figures**

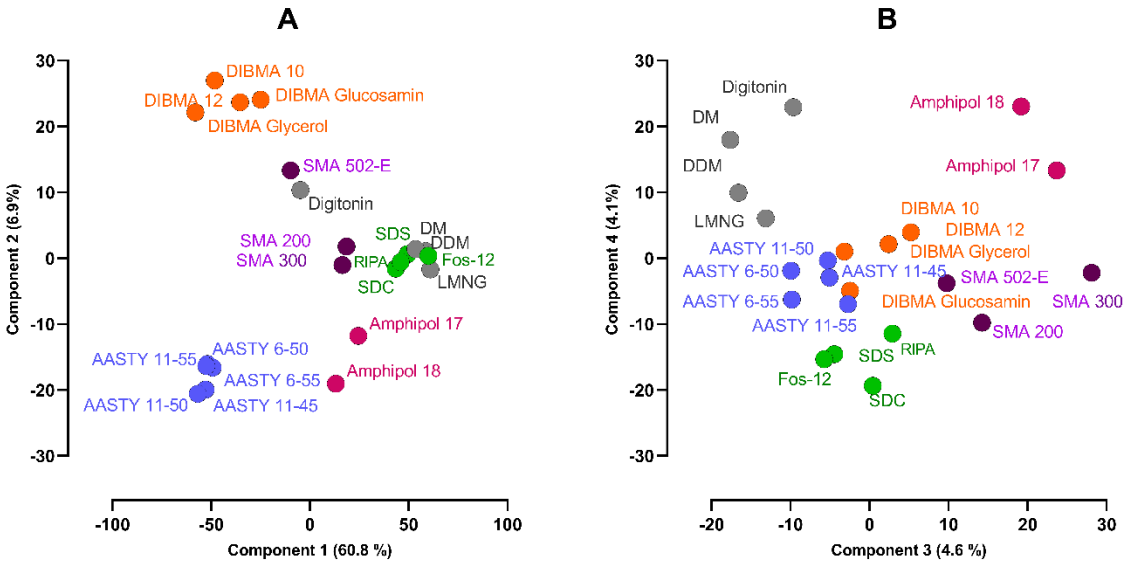

544

545 **Figure 1. Clustering of membrane protein extraction profiles of different solubilization agents.** Principal
546 component analysis of the membrane protein iBAQ values. **A.** Components 1 and 2 of the PCA. **B.**
547 Components 3 and 4. The percentage in each axis label shows the proportinal size of the corresponding
548 eigenvalues. The means of three replicates per extraction condition were used. Each class of
549 solubilization agent is shown in a different color to highlight their clustering.

550

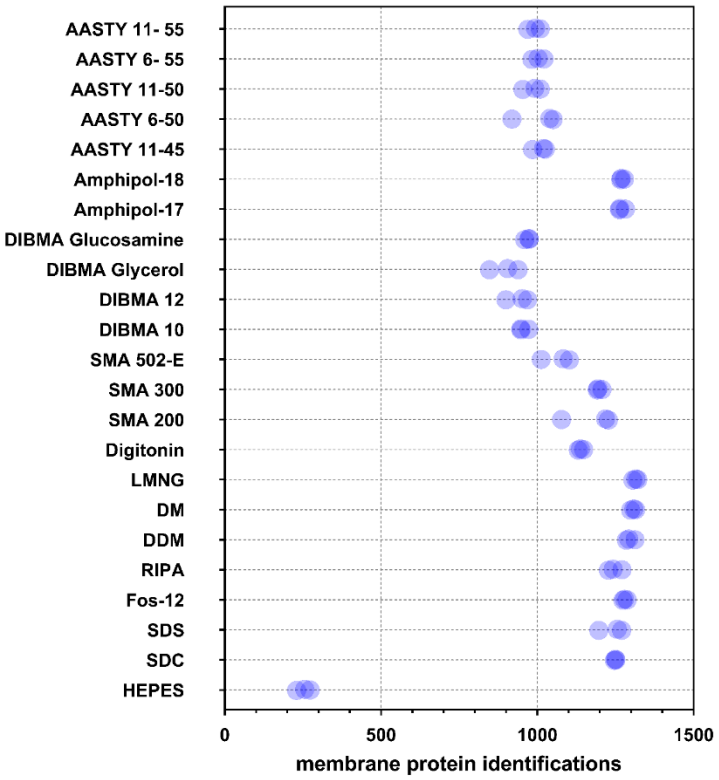

Figure 2. Cumulative number of detected membrane proteins. For each replicate and condition, the sum of membrane protein identifications is shown.

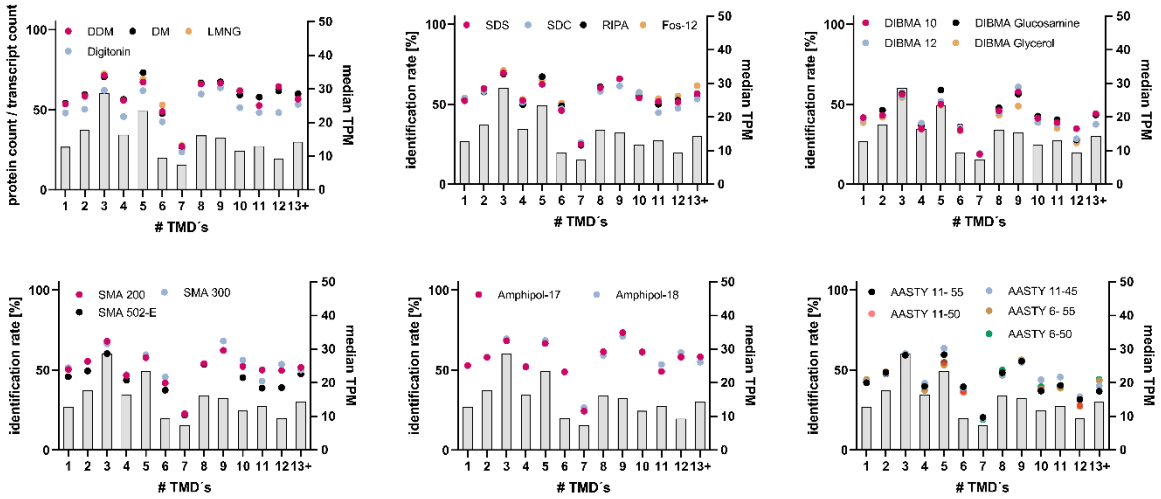

Figure 3. Membrane protein identification rate follows protein abundance in relation to number of TMDs. Proteins were grouped according to their number of transmembrane domains. For each solubilization agent class and each group, the identification rates (colored dots) were calculated as fraction of identified membrane proteins versus the total number of expressed membrane protein transcripts in Hek293 cells in the respective group. For reference, the RNA levels were plotted as median number of TMPs in grey bars.

584

585

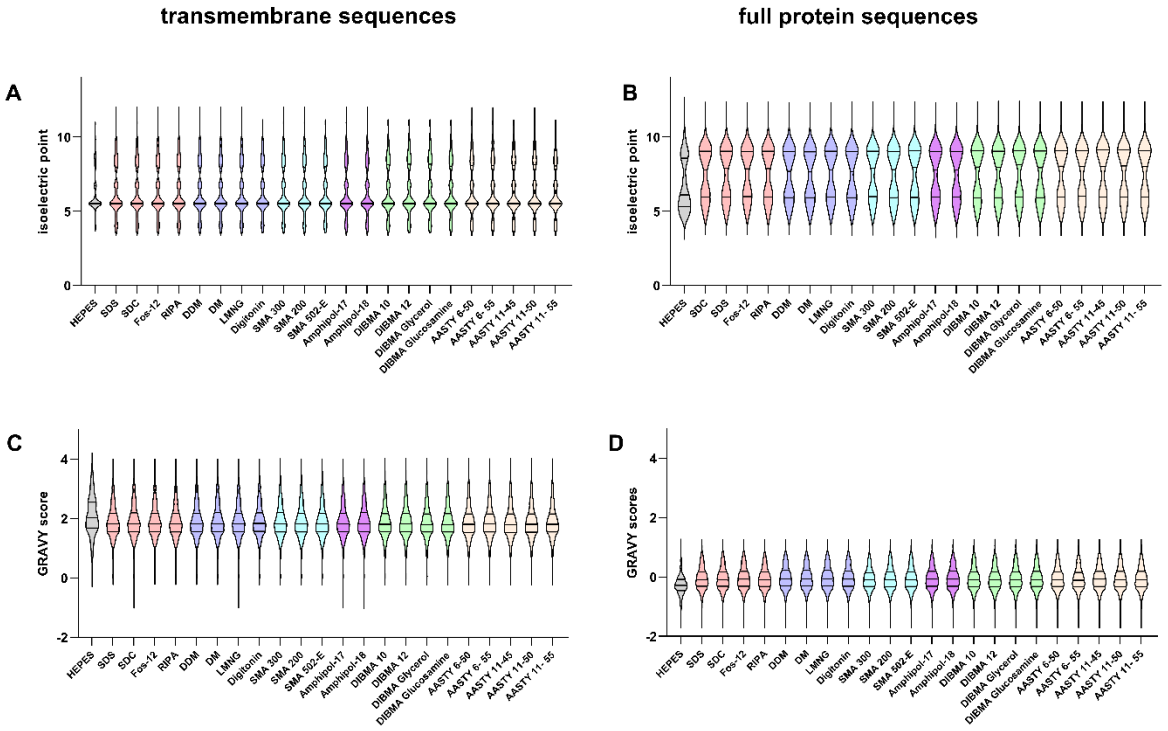

586

587 **Figure 4. Distribution of isoelectric points and GRAVY scores for the proteins detected in solubilization**
588 **experiments.** For all detected membrane proteins, isoelectric points (**A,B**) and GRAVY scores (**C,D**) were
589 calculated using either the transmembrane regions (**A,C**) or the full protein sequence (**B,D**).

590

591

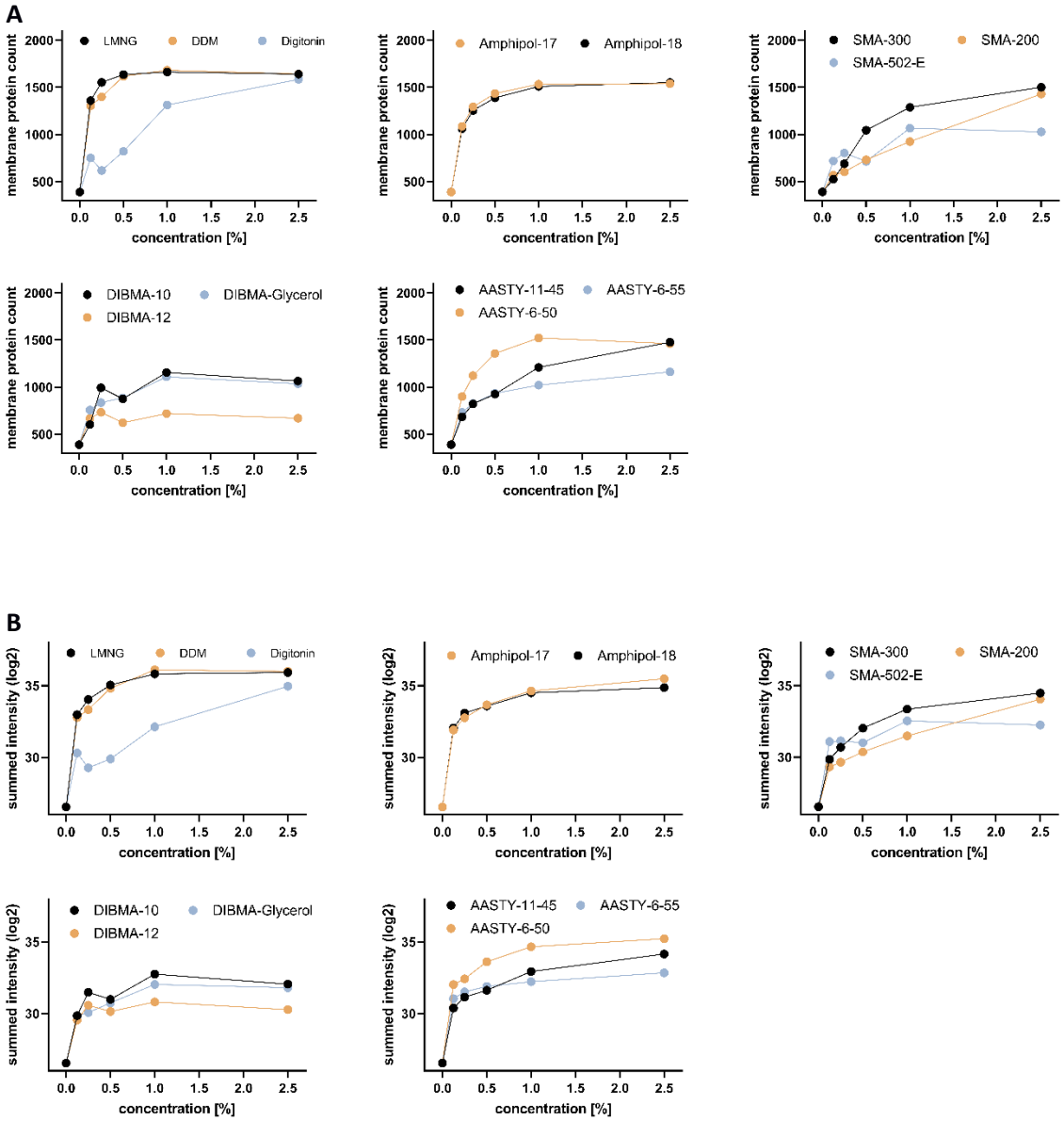

Figure 5. Membrane protein extraction efficiencies of tested solubilization agents. A. Number of unique membrane proteins detected as a function of solubilization agent concentration concentrations (0.125 %, 0.25 %, 0.5 %, 1 %, and 2.5 %). **B.** Summed membrane protein intensities as a function of solubilization agent concentration.

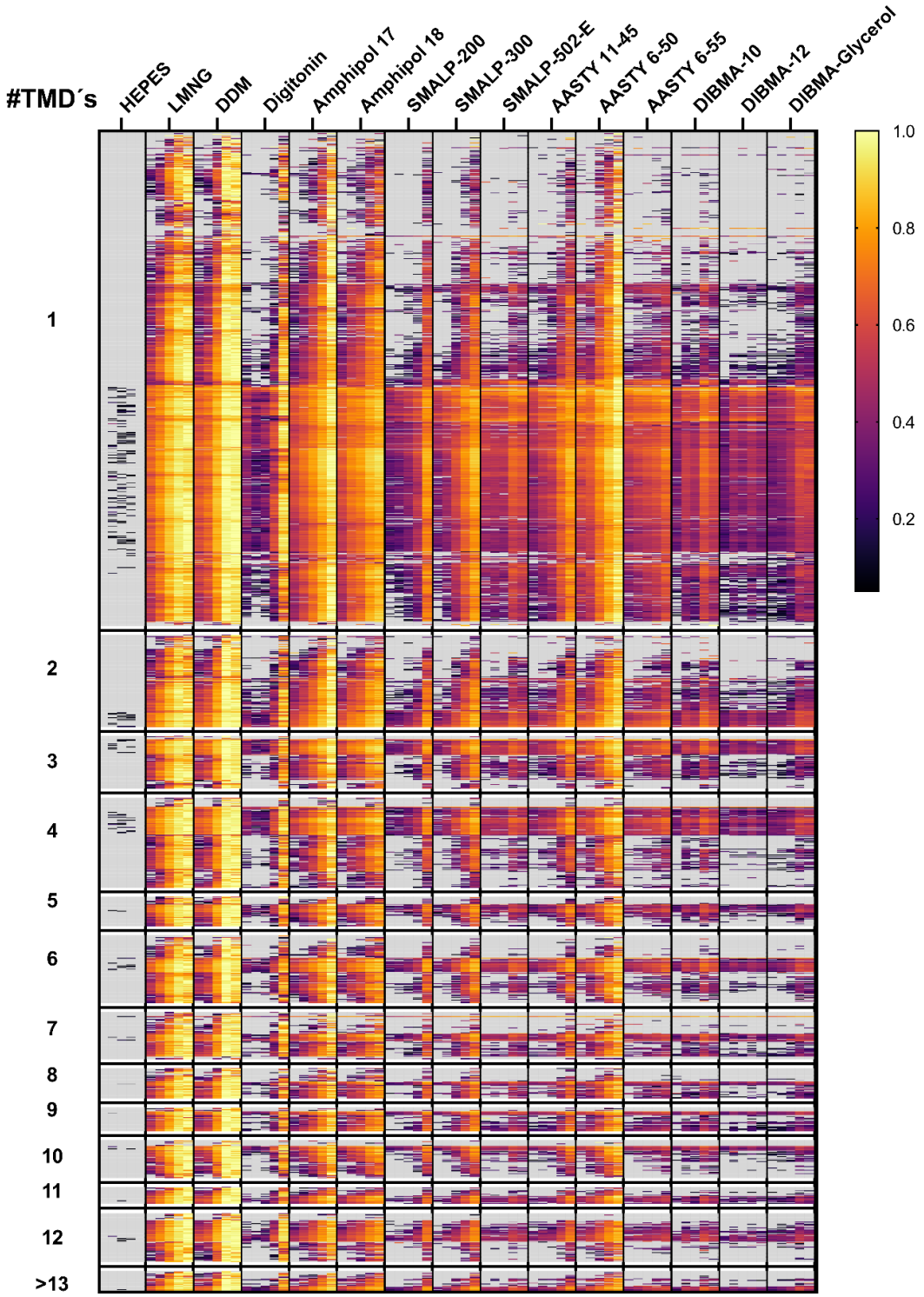

Figure 6. Relative membrane protein intensities in relation to solubilization agent concentrations. For each solubilization agent, five increasing concentrations were tested (0.125 %, 0.25 %, 0.5 %, 1 %, and 2.5 %) and plotted from left to right. HEPES buffer without any additives was used as control in triplicate.

609 Log2 intensities were interval normalised for each row and missing values are displayd in grey. Proteins
610 were grouped according to their number of transmembrane domains as indicated.

611

612 **Table 1.** Summary of the solubilization agents used in our screening experiments.

Class	Copolymer/detergent	Primary screen	Dilution screen
		2.5%	0.125 – 2.5%
AASTY	AASTY 11-55	yes	No
AASTY	AASTY 6-55	yes	Yes
AASTY	AASTY 11-50	yes	No
AASTY	AASTY 6-50	yes	Yes
AASTY	AASTY 11-45	yes	Yes
Amphipol	Ultrasolute™ Amphipol 18 (CyclAPol C8C0-50)	yes	Yes
Amphipol	Ultrasolute™ Amphipol 17 (CyclAPol C6C2-50)	yes	Yes
DIBMA	DIBMA Glucosamine	yes	No
DIBMA	DIBMA Glycerol	yes	Yes
DIBMA	DIBMA 12	yes	Yes
DIBMA	DIBMA 10	yes	Yes
SMA	SMA 502-E	yes	Yes
SMA	SMA 300	yes	Yes
SMA	SMA 200	yes	Yes
Neutral detergents	Digitonin	yes	Yes
Neutral detergents	LMNG	yes	Yes
Neutral detergents	DM	yes	No
Neutral detergents	DDM	yes	Yes
Ionic detergents	RIPA buffer (1 % Nonidet P-40, 0.5 % deoxycholate, 0.1 % SDS)	yes	No
Ionic detergents	SDS	yes, 5%	No
Ionic detergents	SDC	yes	No
Ionic detergents	Fos-12	yes	No
Negative Control	HEPES	yes	Yes

613

614

615 **Supplementary Figure 1 Correspondence between membrane protein mRNA and protein detection in**
616 **Hek293 cells.** RNA transcript counts of membrane protein coding genes were plotted against binned log2
617 transformed TPM. Transcripts with TPM < 1 were removed. In blue, we show the number of proteins we
618 could detect as a function of their corresponding TPM value obtained from Protein Atlas (See methods).

619

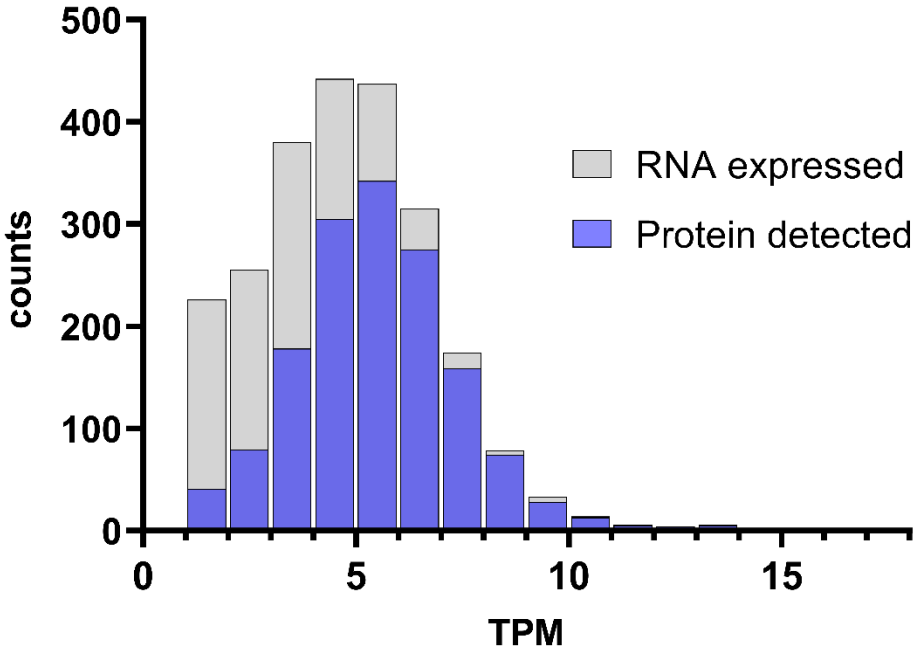

620

621

622

623

624 **Supplementary Table 1. Physicochemical characteristics of all solubilization agents used.**

Copolymer/detergent	Apolar subunit	Polar subunit	Subunit ratio	CMC [% (w/v)]	Mw [g/mol]	Charge	Source
AASTY 11-55	Styrene	Acrylic acid	55:45	n.a.	11,000	Negative	Cube Biotech
AASTY 6-55	Styrene	Acrylic acid	55:45	n.a.	5,500	Negative	Cube Biotech
AASTY 11-50	Styrene	Acrylic acid	1:1	n.a.	11,000	Negative	Cube Biotech
AASTY 6-50	Styrene	Acrylic acid	1:1	n.a.	5,500	Negative	Cube Biotech
AASTY 11-45	Styrene	Acrylic acid	45:55	n.a.	11,000	Negative	Cube Biotech
Ultrasolute Amphipol-18 (CyclAPol C8C0-50)	Cyclooctyl acrylamide	Acrylic acid	1:1	n.a.	7,500	Negative	Cube Biotech
Ultrasolute Amphipol-17 (CyclAPol C6C2-50)	2-Cyclohexyl-ethyl acrylamide	Acrylic acid	1:1	n.a.	7,500	Negative	Cube Biotech
DIBMA Glucosamine	Diisobutylidene	Maleamic acid-glucosamine	1:1	n.a.	14,900	Negative	Cube Biotech
DIBMA Glycerol	Diisobutylidene	Maleamic acid-3-amino-1,2-propanediol	1:1	n.a.	12,500	Negative	Cube Biotech
DIBMA 12	Diisobutylidene	Maleic acid	1:1	n.a.	12,000	Negative	Cube Biotech
DIBMA 10	Diisobutylidene	Maleic acid	1:1	n.a.	10,000	Negative	Cube Biotech
SMA 502-E	Styrene	Maleic acid monoethyl ester	1.5:1	n.a.	7,000	Negative	Cube Biotech
SMA 300	Styrene	Maleic acid	3:1	n.a.	10,000	Negative	Cube Biotech
SMA 200	Styrene	Maleic acid	2:1	n.a.	6,500	Negative	Cube Biotech
Digitonin	n.a	n.a	n.a	0.2 - 0.3	1,229.31	Neutral	Carl Roth
Lauryl maltose neopentyl glycol (LMNG)	n.a	n.a	n.a	0.001	1,005.19	Neutral	Anatrace
Decy-ß-maltoside (DM)	n.a	n.a	n.a	0.087	482.56	Neutral	Cube Biotech
Dodecyl-ß-maltoside (DDM)	n.a	n.a	n.a	0.0087	510.62	Neutral	Cube Biotech
RIPA buffer	n.a	n.a	n.a	n.a.	n.a.	mixed	Sigma-Aldrich
Sodium dodecylsulfat (SDS)	n.a	n.a	n.a	0.2	288.38	Negative	Sigma-Aldrich
Foscholine-12 (Fos-12)	n.a	n.a	n.a	0.047	351.5	Zwitterionic	Cube Biotech
Sodium deoxycholate (SDC)	n.a	n.a	n.a	0.083-0.325	414.55	anionic	Sigma-Aldrich

625

626

627